

# Carbon Monoxide in Comet 9P/Tempel 1 before and after the Deep Impact Encounter<sup>1</sup>

Paul D. Feldman,<sup>2</sup> Roxana E. Lupu,<sup>2</sup> Stephan R. McCandliss,<sup>2</sup> Harold A. Weaver,<sup>3</sup>  
Michael F. A'Hearn,<sup>4</sup> Michael J. S. Belton,<sup>5</sup> and Karen J. Meech<sup>6</sup>

## ABSTRACT

One of the goals of the *Hubble Space Telescope* program to observe periodic comet 9P/Tempel 1 in conjunction with NASA's Deep Impact mission was to study the generation and evolution of the gaseous coma resulting from the impact. For this purpose, the Solar Blind Channel of the Advanced Camera for Surveys was used with the F140LP filter which is sensitive primarily to the ultraviolet emission ( $\geq 1400\text{\AA}$ ) from the CO Fourth Positive system. Following the impact we detected an increase in brightness, which if all due to CO corresponds to  $1.5 \times 10^{31}$  molecules or a mass of  $6.6 \times 10^5$  kg, an amount that would normally be produced by 7–10 hours of quiescent outgassing from the comet. This number is  $\leq 10\%$  of the number of water molecules excavated, and suggests that the volatile content of the material excavated by the impact did not differ significantly from the surface or near sub-surface material responsible for the quiescent outgassing of the comet.

*Subject headings:* comets: individual (9P/Tempel 1) — ultraviolet: solar system

---

<sup>1</sup>Based on observations with the NASA/ESA *Hubble Space Telescope* obtained at the Space Telescope Science Institute, which is operated by the Association of Universities for Research in Astronomy (AURA), Inc., under NASA contract NAS 5-26555.

<sup>2</sup>Department of Physics and Astronomy, The Johns Hopkins University, Charles and 34th Streets, Baltimore, MD 21218, pdf@pha.jhu.edu, roxana@pha.jhu.edu, stephan@pha.jhu.edu

<sup>3</sup>Space Department, Johns Hopkins University Applied Physics Laboratory, 11100 Johns Hopkins Road, Laurel, MD 20723-6099, hal.weaver@jhuapl.edu

<sup>4</sup>Department of Astronomy, University of Maryland, College Park MD 20742-2421, ma@astro.umd.edu

<sup>5</sup>Belton Space Exploration Initiatives, Tucson, AZ 85716, mbelton@dakotacom.net

<sup>6</sup>University of Hawaii, Institute for Astronomy and NASA Astrobiology Institute, 2680 Woodlawn Drive, Honolulu, HI 96822, meeck@ifa.hawaii.edu

## 1. INTRODUCTION

The Deep Impact mission (A'Hearn et al. 2005a,b) successfully placed a 364 kg impactor, onto the surface of comet 9/P Tempel 1 at a relative velocity of  $10.3 \text{ km s}^{-1}$  on 2005 July 4 at 05:52:03 UT (as seen from Earth). The event was observed by cameras aboard the mother spacecraft and by a large number of Earth- and space-based telescopes as part of an extensive campaign to study the comet prior to, during, and in the course of several days following the impact (Meech et al. 2005). The *Hubble Space Telescope (HST)* provided the highest spatial resolution images (36 km) from Earth using the Advanced Camera for Surveys (ACS) High Resolution Channel (HRC), and also the possibility of using ultraviolet spectroscopy to study the evolution of gaseous species, particularly CO, released by the impact. The latter was initially planned for the Space Telescope Imaging Spectrograph (STIS), but after the failure of STIS in August 2004, was replaced with filter and prism observations using the Solar Blind Channel (SBC) of ACS. This paper presents the results of the SBC observations and an estimate of the amount of CO released in the gaseous ejecta. A discussion of the visible imaging results is given by Feldman et al. (2006).

## 2. OBSERVATIONS

The *HST* campaign consisted of 17 separate “visits” during 2005 June and July, each comprising a single *HST* orbit allowing  $\sim$ 53 minutes of target visibility per orbit. The July program (ID 10456) was divided into three periods: a pre-impact group beginning roughly one cometary rotation before impact to establish a baseline for the data to follow; the *HST* orbit that included the impact time; and several orbits immediately following the impact and continuing, with single orbits, 7 and 12 days after the impact. Because of the large overhead in switching cameras during a single *HST* orbit, entire visits were dedicated to the SBC observations. These included two orbits prior to impact and three within the 24 hour period following impact, which it turns out were sufficient to see the ultraviolet brightness of the coma return to its quiescent level. The observations were made with both a long-pass filter (F140LP) that is sensitive primarily to the ultraviolet emission from the Fourth Positive system of carbon monoxide, and with the largely unused objective prism PR130L. The filter has a peak throughput at  $1390 \text{ \AA}$  and half-power points at  $1362$  and  $1584 \text{ \AA}$ .<sup>7</sup> Because of the low count rate of the data, the prism data are difficult to interpret, and in the following we will focus only on the images obtained with the long-pass filter. A log of the images is

---

<sup>7</sup>see the ACS Instrument Handbook available at  
[http://www.stsci.edu/hst/acs/documents/handbooks/cycle15/c10\\_ImagingReference41.html#317506](http://www.stsci.edu/hst/acs/documents/handbooks/cycle15/c10_ImagingReference41.html#317506)

given in Table 1.

### 3. ULTRAVIOLET IMAGING

#### 3.1. Data Analysis

The SBC is an ultraviolet imager with a field-of-view of  $31'' \times 35''$  and a plate scale of  $0.''032 \text{ pixel}^{-1}$ . Like the ACS CCD channels (described by Sirianni et al. 2005), the SBC focal plane array, consisting of a multianode microchannel plate array (MAMA) detector, is tilted with respect to the incoming rays. This leads to significant geometric distortion that is corrected in the calibration pipeline processing. The resulting asymmetric array contains the data resampled into  $0.''025 \times 0.''025$  pixels. The pipeline also subtracts a calibration dark count flat field image, and there is no appreciable sky background with the F140LP filter. A first inspection of the F140LP images reveals no concentrated source of emission at the expected position of the comet. It is only with significant rebinning of the geometrically corrected images into  $16 \times 16$  superpixels (each of size  $0.''4 \times 0.''4$ ) that the structure of the coma emerges. The rebinned image taken 2.69 hr after the impact is shown in Figure 1.

##### 3.1.1. Radial Profiles and Light Curves

The centroid of each image is located and aperture photometry is extracted with circular apertures of 1, 2, 4, 10 and 16 arc seconds. Radial profiles of the emission are extracted by averaging circular annuli of 1 pixel width over a full  $2\pi$  radians. Directional information is lost because of the very low count rate. The radial profiles are shown in Figure 2, in which the data from the two pre-impact images are combined to enhance the signal-to-noise ratio of the image.

The temporal evolution of the gas coma is illustrated by the figure. The visit 07 image, 2.69 hr after impact, shows an enhancement in the inner coma with the radial profile returning to the quiescent level  $9.''5$  from the center of brightness. Assuming that the CO, like the ejected dust, is produced in a time short compared to the time after impact (A'Hearn et al. 2005b), then this distance translates to a maximum component of outflow velocity of  $\sim 700 \text{ m s}^{-1}$ . There is also evidence, in the form of a shelf extending out  $1.''5$  from the center of brightness, of a slower component with a velocity of  $\sim 100 \text{ m s}^{-1}$ , perhaps CO released from slower moving small grains excavated by the impact. However, this only represents  $\sim 10\%$  of the new material in the field-of-view. The visit 09 image, 5.99 hr after impact, shows the profile decreasing in the inner region but extending to greater distances from the

nucleus as the gas continues to expand away from the nucleus. The final image, from visit 11, 20.29 hr after impact, shows the gas returning to its pre-impact level.

This behavior may also be illustrated with light curves derived from the aperture photometry, as shown in Figure 3. The data are plotted as the ratio of the count rate to that of the pre-impact average and for the three apertures shown the increase ranges from a factor of 1.8 (1'') to 1.5 (4''). Despite the paucity of data samples, the points for visits 07 and 09 can be fit approximately with exponentials of time constant ranging from 3.0 hr (1'') to 6.5 hr (4'').

### 3.1.2. Filter Calibration

It is necessary to turn the observed count rate to a measure of CO column density in the field-of-view. From observations of many comets by sounding rockets, *IUE*, and *HST*, the bandpass of the F140LP filter contains primarily emissions of C I and the Fourth Positive system ( $A^1\Pi - X^1\Sigma^+$ ) of CO, with some additional weaker emissions, dependent on heliocentric velocity, of S I (Feldman et al. 2004). The atomic carbon emissions, being dissociation products of long lived species, have a flat spatial distribution near the nucleus that is seen in *HST* Space Telescope Imaging Spectrograph long-slit spectra (over a 25'' field) of several comets (Weaver et al. 2002). On the other hand, the CO, except for optical depth effects close to the nucleus, largely follows the inverse square density distribution of a parent molecule. For the quiescent images we assume that the spatially varying component of the image is due solely to CO emission.

To calibrate the filter we calculate the effective transmission of the CO Fourth Positive system as follows. We begin with a fluorescence model of the band system that was developed to model STIS spectra of several comets taking into account saturation of the solar radiation field and self absorption along the line of sight to the observer (Lupu et al. 2004). For a given CO column density the calculated line-by-line brightness of the band is multiplied by the filter transmission at each wavelength to obtain an effective fluorescence efficiency. The images, which are given in counts  $s^{-1}$  per pixel, are then converted into column density per pixel.

This process is validated using data from an ACS GTO program (ID 9985) that observed comet C/2002 T7 (LINEAR) on 2004 June 5. That program included observations with two long-pass filters, F140LP and F165LP, and with STIS, the latter to provide information about the spectral content in the bandpass of the filters. The difference images, subtracting the F165LP image from F140LP, then span a wavelength range that matches closely the

long wavelength range of the STIS G140L grating. Using the two sets of data independently to derive a CO production rate yields results that agree to better than 30% of each other (Feldman et al., in preparation). While we cannot be certain that the spectral content of 9P/Tempel 1 is the same as that of C/2002 T7, particularly the content of the ejecta, within these caveats we can reliably derive the amount of CO in the coma of 9P/Tempel 1 before and following the impact. Even so, it is difficult to imagine any other species produced by the impact, such as N<sub>2</sub>, that might fluoresce strongly in the filter bandpass.

### 3.2. Quiescent Production Rate

From the mean of the two pre-impact images, a radial outflow model, together with the effective fluorescence efficiencies described above, is used to model the CO vaporized from a point-like nucleus. The only independent parameter is the outflow velocity, which we take to be the canonically used H<sub>2</sub>O outflow velocity,  $0.85r^{-0.5}$  km s<sup>-1</sup>, where  $r$  is the heliocentric distance in AU (Budzien et al. 1994). Even at the edges of the approximately 30"  $\times$  34" SBC field-of-view the observed count rate does not decrease to the detector background level because of the atomic carbon emissions present in the filter bandpass. We attempt to model the radial profile with different assumptions to constrain the level of the uniform background emissions. The results are shown in Figure 4, and constrain the quiescent production rate to  $Q(\text{CO}) = 4 - 6 \times 10^{26}$  molecules s<sup>-1</sup>. We do not consider the possibility that some of the observed CO is the result of the dissociation of either CO<sub>2</sub> or H<sub>2</sub>CO.

### 3.3. CO Abundance in Ejecta

The evaluation of the amount of CO in the ejecta is both easier and more difficult than the quiescent case. We noted that the radial profile for visit 07 (Fig. 2) appeared enhanced over the pre-impact profiles only out to a radial distance of 9.5". We can then integrate the difference between the column densities derived for this image and those for the pre-impact images to determine the total CO content added to the coma. The difficulty is the assumption that all of the emission is due to CO, but with that assumption we derive a total number of molecules of  $1.5 \times 10^{31}$  molecules or a mass of  $6.6 \times 10^5$  kg. This result is somewhat model dependent although the CO column densities are for the most part too small for unity optical depth in absorption to be reached. Because the photodissociation lifetime of CO is greater than 10<sup>6</sup> s at 1 AU (Huebner et al. 1992), the amount of atomic carbon added to the coma by this process in  $\sim$ 3 hr is small and does not contribute to the observed emission. However, we cannot exclude the possibility of atomic sulfur produced

from short-lived parents such as  $\text{H}_2\text{S}$ ,  $\text{CS}_2$ , or  $\text{S}_2$ , or of other “organic” sources of CO or C. The infrared spectrometer on Deep Impact recorded a large increase following impact in emission at  $\sim 3.5 \mu\text{m}$ , attributed to a C–H stretching vibration of some simple organic molecules, and also in  $\text{CO}_2$  (A’Hearn et al. 2005b), so that some of the observed CO could result from elevated levels of  $\text{CO}_2$  or  $\text{H}_2\text{CO}$  in the ejecta. The derived abundance must thus be regarded as an upper limit to the amount of CO produced by the excavation. Relative to the quiescent CO production rate given above, the added material corresponds to 7–10 hr of natural outgassing over the entire surface of the comet.

#### 4. DISCUSSION

It is of interest to know how the CO/ $\text{H}_2\text{O}$  abundance in the excavated material compares with that found in normal cometary outgassing. We did not have the means to simultaneously determine the water production rate with *HST*, and the reports currently in the literature based on different techniques are somewhat divergent. These are summarized in Table 2. Küppers et al. (2005) analyzed narrow-band OH images recorded by the OSIRIS cameras on board the *Rosetta* spacecraft, and used a Haser model with a parent outflow velocity similar to that used above for CO to obtain the quiescent production rate. Schleicher et al. (2006) obtained a production rate from ground-based OH photometry, and only a limit for the total post-impact production. Mumma et al. (2005) estimated the pre-impact production rate from infrared long-slit spectroscopy, and because their long slit did not include all of the water produced by the impact, report only an effective post-impact production rate which is twice their quiescent value. The results of Biver et al. (2005) are from the *Odin* satellite, observing at 557 GHz.

The pre-impact CO/ $\text{H}_2\text{O}$  value presented in Table 2 uses the two largest water production rates, both of which are based on direct observations of  $\text{H}_2\text{O}$ . The derived value, 4–6%, appears to be relatively high for a Jupiter family comet, but is well within the range of values (<0.4–30%) of several recent comets (Bockelée-Morvan et al. 2004). We note that existing radio observations do not provide a reliable constraint on the CO abundance of Jupiter family comets (Biver et al. 2002).

Combining the  $\text{H}_2\text{O}$  measurements post-impact with our CO abundance yields a derived CO/ $\text{H}_2\text{O}$  ratio <10%. Thus, it appears that the CO/ $\text{H}_2\text{O}$  abundance ratio in the excavated material is not significantly larger than in the surface material, *i.e.*, the impact did not excavate a region of buried highly volatile ices. Our result is consistent with the findings of Sunshine et al. (2006) from Deep Impact images that  $\text{H}_2\text{O}$  ice deposits on the surface of the comet are insufficient to account for the ambient outgassing rate of the comet. They

postulate extensive sub-surface sources of ice, and it appears that the excavation of such material is also producing a brief enhancement in CO following the impact.

We note that Mumma et al. also observed CO following the impact (they did not measure it pre-impact), and derive a column abundance relative to H<sub>2</sub>O in their long slit of 4.3%, which is consistent with our result. However they get the same values for the amount of CO in their slit both 1.8 hr and 24 hr after impact, a result incompatible with our light curve (Fig. 3). Biver et al. (2005) also report pre- and post-impact upper limits on CO from ground-based radio observations, but these are 3–4 times higher than our result.

## 5. CONCLUSION

Observations of comet 9P/Tempel 1 made by the Solar Blind Channel of the ACS on *HST* have provided unique estimates of the CO content of the coma both before and after the Deep Impact encounter. Despite the low ultraviolet flux from the comet, the observation was made possible by the high ultraviolet throughput of the SBC and by integration of a major fraction of the CO Fourth Positive emissions in the bandpass of the F140LP filter. The abundance of CO relative to H<sub>2</sub>O remains uncertain because of the spread in the values of H<sub>2</sub>O reported to date and the uncertain contribution of C I to the observed count rate, but to within the present uncertainties appears to be the same in the ejecta as in the quiescent coma. This situation should improve upon further analysis and with additional data. However, it is clear that the impact did not produce ejecta derived primarily from highly volatile ices.

We thank Ian Jordan, Ron Gilliland, and Charles Proffitt (STScI) for the planning and successful execution of the *HST* program; Eddie Bergeron, Max Mutchler, Zolt Levay (STScI) and Ken Anderson (JHU) for the rapid response and production of properly corrected images; Cheryl Gundy, Lisa Frattare, Ray Villard, Mario Livio, and countless others at STScI for the July 4 logistics; and STScI/JPL for coordination of impact time before the end of *HST* visibility. This work was supported by grant GO-10144.01-A from the Space Telescope Science Institute.

## REFERENCES

A'Hearn, M. F., Belton, M. J. S., Delamere, A., & Blume, W. H. 2005a, Space Science Reviews, 117, 1

A'Hearn, M. F., et al. 2005b, Science, 310, 258

Biver, N., et al. 2002, *Earth Moon and Planets*, 90, 323

Biver, N., et al. 2005, *BAAS*, 37, 710

Bockelée-Morvan, D., Crovisier, J., Mumma, M. J., & Weaver, H. A. 2004, in *Comets II*, ed. M. C. Festou, H. A. Weaver, & H. U. Keller (Tucson: Univ. of Arizona), 391

Budzien, S. A., Festou, M. C., & Feldman, P. D. 1994, *Icarus*, 107, 164

Feldman, P. D., Cochran, A. L., & Combi, M. R. 2004, in *Comets II*, ed. M. C. Festou, H. A. Weaver, & H. U. Keller (Tucson: Univ. of Arizona), 425

Feldman, P. D., McCandliss, S. R., Route, M., Weaver, H. A., A'Hearn, M. F., Belton, M. J. S., & Meech, K. J. 2006, *Icarus*, in press

Huebner, W. F., Keady, J. J., & Lyon, S. P. 1992, *Solar photo rates for planetary atmospheres and atmospheric pollutants* (Dordrecht; Boston: Kluwer Academic)

Küppers, M., et al. 2005, *Nature*, 437, 987

Lupu, R. E., Feldman, P. D., Weaver, H. A., & Tozzi, G.-P. 2004, *BAAS*, 36, 1433

Meech, K. J., et al. 2005, *Science*, 310, 265

Mumma, M. J., et al. 2005, *Science*, 310, 270

Schleicher, D. G., Barnes, K. L., & Baugh, N. F. 2006, *AJ*, 131, 1130

Sirianni, M., et al. 2005, *PASP*, 117, 1049

Sunshine, J. M., et al. 2006, *Science*, 311, 1453

Weaver, H. A., Feldman, P. D., A'Hearn, M. F., Arpigny, C., Combi, M. R., Festou, M. C., & Tozzi, G.-P. 2002, *BAAS*, 34, 853

Table 1: Summary of ACS/Solar Blind Channel F140LP images of comet 9P/Tempel 1.  $r$  and  $\Delta$  are heliocentric and geocentric distances, respectively.

Visit	Image	Exposure	Date	Start	Time From	$r$	$\Delta$	Phase
	ID	Time (s)		Time (UT)	Impact <sup>a</sup> (hr)	(AU)	(AU)	Angle (°)
02	J9A802EAQ	509.0	2005-07-02	02:07:50	−51.67	1.507	0.883	40.7
04	J9A804IGQ	509.0	2005-07-03	00:30:59	−29.28	1.506	0.888	40.8
07	J9A807F1Q	460.0	2005-07-04	08:29:53	2.69	1.506	0.895	41.0
09	J9A809FKQ	380.0	2005-07-04	11:48:09	5.99	1.506	0.895	41.0
11	J9A811IYQ	509.0	2005-07-05	02:05:20	20.29	1.506	0.898	41.0

<sup>a</sup>Exposure mid-point.

Table 2: Pre- and post-impact H<sub>2</sub>O and CO abundances.

Period	H <sub>2</sub> O <sup>a</sup>	Reference <sup>b</sup>	CO <sup>a</sup>	Reference <sup>b</sup>	CO/H <sub>2</sub> O
Pre-impact	$10.4 \times 10^{27}$	1	$4 - 6 \times 10^{26}$	5	$4 - 6\%$
	$(8.5 \pm 1.5) \times 10^{27}$	2			
	$6 \times 10^{27}$	3			
	$(3.4 \pm 0.5) \times 10^{27}$	4			
Post-impact	$(1.4 \pm 0.35) \times 10^{32}$	2	$1.5 \times 10^{31}$	5	$< 10\%$
	$< 4 \times 10^{32}$	3			
	$(1.5 \pm 0.5) \times 10^{32}$	4			

---

<sup>a</sup>Pre-impact production rates in molecules s<sup>-1</sup>; post-impact abundances in molecules.

<sup>b</sup>REFERENCES.— (1) Mumma et al. 2005; (2) Biver et al. 2005; (3) Schleicher et al. 2006; (4) Kuppers et al. 2005; (5) This paper.

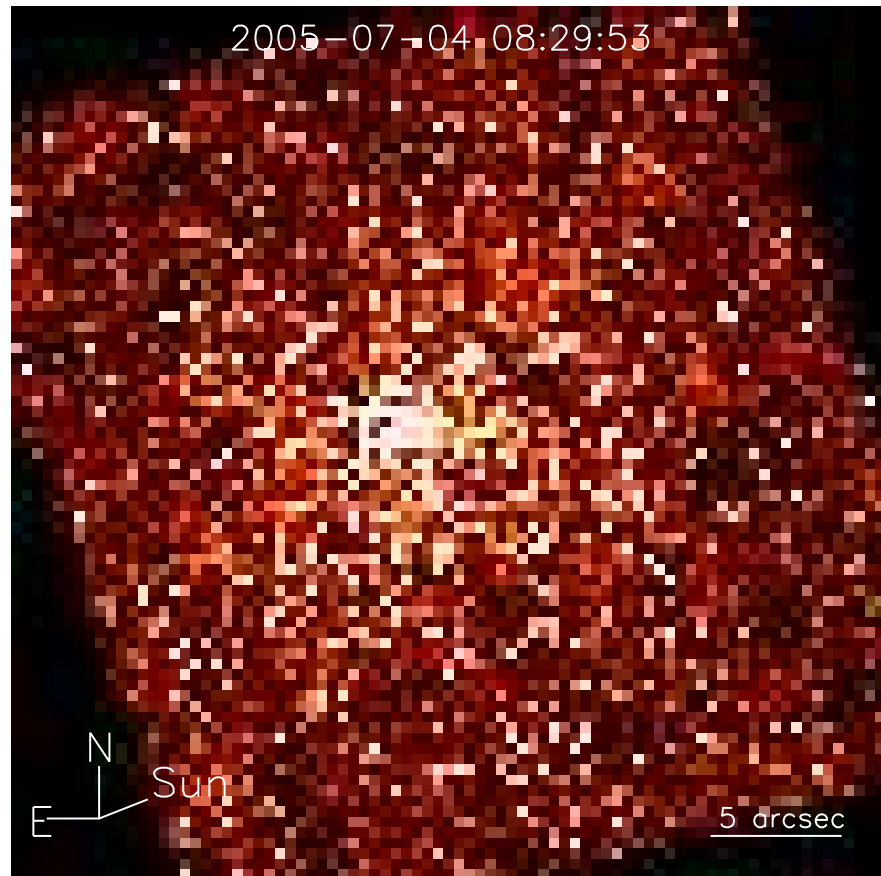


Fig. 1.— F140LP image of comet 9P/Tempel 1 taken 2.69 hr after the impact. The image has been geometrically corrected and rotated and then rebinned to  $0.^{\prime\prime}4 \times 0.^{\prime\prime}4$  pixels. The exposure start time is given on the image.

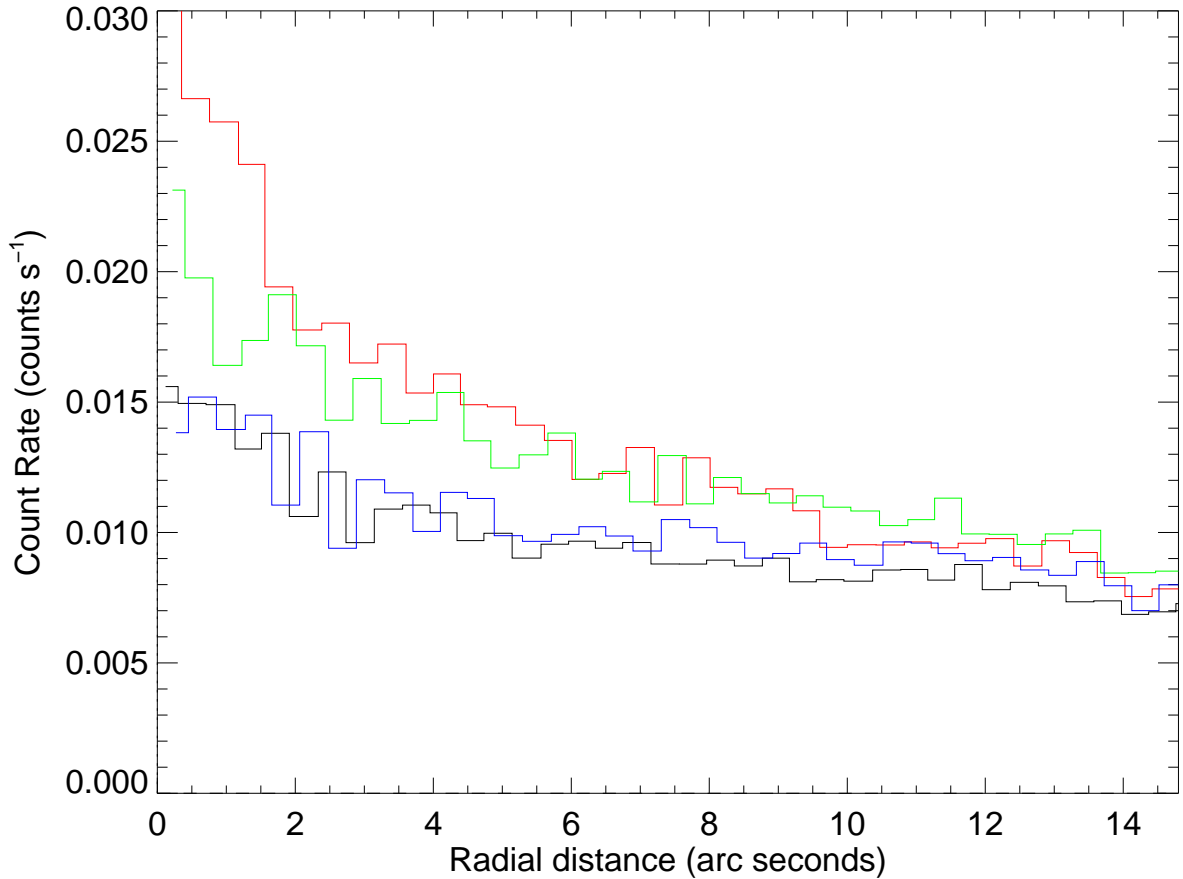


Fig. 2.— Radial profiles of the observed ultraviolet emission derived from images processed as in Fig. 1. The profiles are obtained by averaging circular annuli in widths of 1 pixel ( $0.^{\prime\prime}4$ ) about the center of brightness. Black: average of pre-impact (visits 02 and 04) images; red: 2.69 hr after impact; green: 5.99 hr after impact; blue: 20.29 hr after impact.

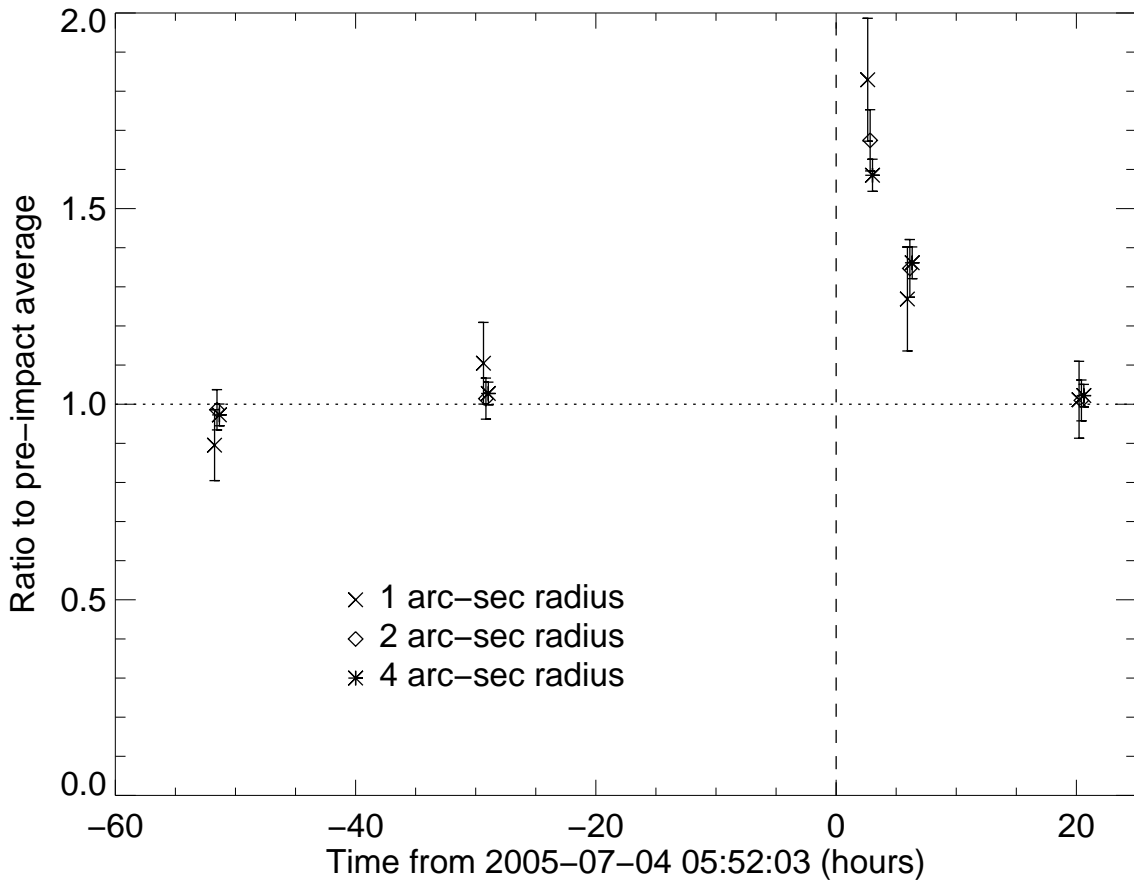


Fig. 3.— Light curves of the ultraviolet emission obtained by summing the count rate in three different circular apertures. The intensities are plotted as the ratio to the average of the two pre-impact values.

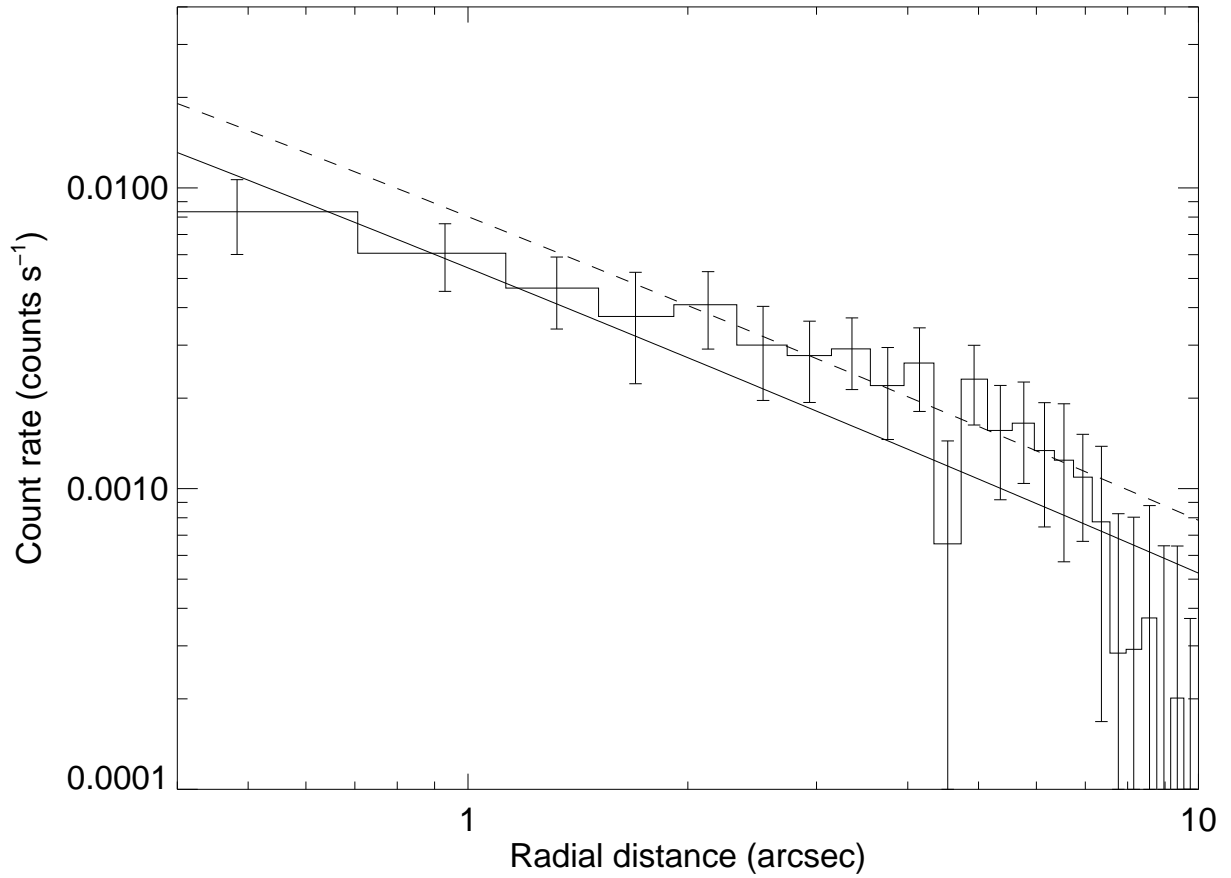


Fig. 4.— Pre-impact radial profile together with CO fluorescence models that constrain the quiescent CO production rate. A uniform background of  $0.0083 \text{ counts s}^{-1}$  has been subtracted from the data shown in Fig. 2. Solid line:  $Q(\text{CO}) = 4.0 \times 10^{26} \text{ molecules s}^{-1}$ ; Dashed line:  $Q(\text{CO}) = 6.0 \times 10^{26} \text{ molecules s}^{-1}$ .